Labeling strategy to improve neutron/gamma discrimination with plastic scintillator using artificial neural network

Ali Hachem, Yoann Moline, Gwenolé Corre, Bassem Ouni, Mathieu Trocme, Aly Elayeb, Frédérick Carrel

Nuclear Engineering and Technology xxx (xxxx) xxx

Contents lists available at ScienceDirect

Nuclear Engineering and Technology

journal homepage: www.elsevier.com/locate/net

Original article

Labeling strategy to improve neutron/gamma discrimination with organic scintillator

Ali Hachem *, Yoann Moline, Gwenolé Corre, Bassem Ouni, Mathieu Trocme, Aly Elayeb, Frédérick Carrel

Paris-Saclay University, CEA, List, Saclay, France

ARTICLE INFO

Keywords:
Neutron gamma discrimination
Time-of-flight
Labeling approach
Plastic scintillator
Organic scintillator
Machine learning

ABSTRACT

Organic scintillators are widely used for neutron/gamma detection. Pulse shape discrimination algorithms have been commonly used to discriminate the detected radiations. These algorithms have several limits, in particular with plastic scintillator which has lower discrimination ability, compared to liquid scintillator. Recently, machine learning (ML) models have been explored to enhance discrimination performance. Nevertheless, obtaining an accurate ML model or evaluating any discrimination approach requires a reference neutron dataset. The preparation of this is challenging because neutron sources are also gamma-ray emitters. Therefore, this paper proposes a pipeline to prepare clean labeled neutron/gamma datasets acquired by an organic scintillator. The method is mainly based on a Time of Flight setup and Tail-to-Total integral ratio (TTT_{ratio}) discrimination algorithm. In the presented case, EJ276 plastic scintillator and ^{252}Cf source were used to implement the acquisition chain. The results showed that this process can identify and remove mislabeled samples in the entire ToF spectrum, including those that contribute to peak values. Furthermore, the process cleans ToF dataset from pile-up events, which can significantly impact experimental results and the conclusions extracted from them.

1. Introduction

The detection of neutron radiations by organic scintillators (plastic, liquid and stilbene) has many applications in several fields such as homeland security and nuclear medicine. These scintillators are also sensitive to gamma-rays. Moreover, the emission of neutrons is always accompanied by an emission of gamma-rays. Pulse shape discrimination techniques, such as zero crossing [1], TTT_{ratio} integral ratio [2] and curve-fitting [3] have been proposed to discriminate the neutron events from the detected gamma-rays. These algorithms rely on the difference in shape of the signals to classify them. Neutron interaction produces a longer signal than the one generated by gamma-ray [4].

This difference is more important in liquid and stilbene organic scintillators. Thus, the discrimination ability of these detectors is higher compared to their plastic counterparts using pulse shape discrimination algorithms [5–8]. However, despite this intrinsic limitation, plastic organic scintillators have several advantages. They can be easily produced and have a relatively low cost [9]. In addition, they have increased durability, non-toxicity, and non-flammability characteristics. In recent years, Eljen Technology has developed a commercial pulse shape discriminating plastic scintillator (EJ276) [10]. Its pulse shape discrimination properties have increased to be comparable to those offered by liquid scintillators. Fig. 1 shows the difference between the average neutron and gamma-ray signals produced by EJ276 plastic scintillator

Recently, machine learning (ML) techniques have been explored to improve discrimination performance with liquid and stilbene scintillators [11–14]. The authors of [11] propose a non negative matrix factorization to discriminate neutron gamma radiations with stilbene scintillator. Another study proposes a Gaussian Mixture model with EJ309 liquid scintillator [12]. However, both studies do not show how the pure neutron and gamma signals were prepared to evaluate the methods. In [13,14], the authors implement an artificial neutral network (ANN) and Support Vector Machine models to achieve the discrimination with stilbene and liquid scintillator, respectively. Another ML model is proposed in [15] to classify radiations detected by the EJ299-33 plastic scintillator. While the discrimination performance is improved in the three previous studies, the ML models were trained on datasets labeled by TTT_{ratio} discrimination algorithm. The accuracy of the labeling by this algorithm is decreased when dealing with relatively low energy radiations due to a significant overlap between the TTT_{ratio} distributions of neutrons and gamma-rays [16]. Choosing one TTT_{ratio}

* Corresponding author.
E-mail address: ali.hachem@cea.fr (A. Hachem).

https://doi.org/10.1016/j.net.2023.07.024
Received 25 October 2022; Received in revised form 18 July 2023; Accepted 19 July 2023
Available online 24 July 2023

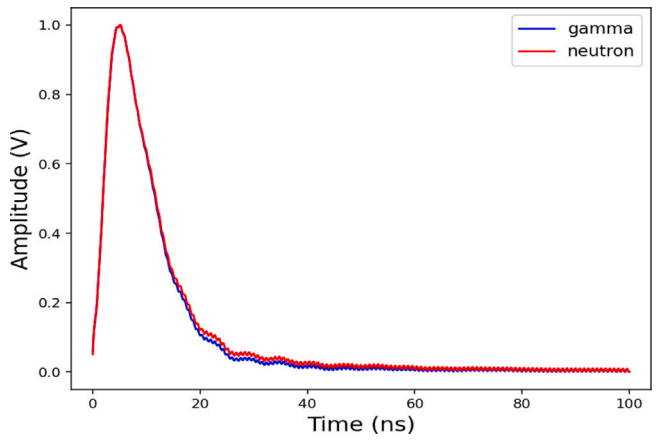

Fig. 1. Average of neutron and gamma-ray signals detected by EJ276 plastic scintillator.

threshold to classify the signals results to a significant number of mislabeled samples.

Despite the results obtained by all previous work on the neutron gamma discrimination task, obtaining an accurate ML model or the evaluation of any discrimination approach remains a difficult task due to the lack of a reference neutron dataset. The main limitation for obtaining this dataset is the impact of gamma-rays emissions in neutron sources.

This paper proposes a pipeline to prepare clean and labeled neutron/gamma datasets detected by an organic scintillator (Fig. 2). First, a dataset is acquired using Time of Flight (ToF) experimental setup. Then, the acquired dataset is cleaned up from pile-up events. Thereafter, the remaining signals are processed to decrease the number of background events, they are then labeled based on ToF information. The last step is identifying and removing the mislabeled samples obtained by ToF using a proposed labeling method based on TTT_{ratio} algorithm. Furthermore, the article shows the results provided by a proof of concept ANN model trained on the prepared dataset. The results are compared to those obtained by TTT_{ratio} discrimination algorithm.

In Section 2 we will explain in details the ToF and standard experimental setup that we built to prepare the real neutron/gamma datasets. The radioactivity sources used in these acquisition chains are ^{252}Cf and ^{60}Co. Then, in Section 3 we will introduce the pile-up detection algorithm that we implemented to clean up the data acquired by ToF setup. Section 4 explains the proposed strategy to remove the mislabeled samples. The method depends on the results obtained by the ToF experiment and TTT_{ratio} discrimination algorithm. Recently, a similar approach has been proposed to remove the mislabeled samples in the dataset acquired by ToF setup using EJ309 liquid organic scintillator [17]. However, the energy distributions of classified neutron and gamma-rays do not correspond to the chosen thresholds to remove the mislabeled samples.

In Section 5 the paper shows the results obtained after training of an ANN model on the prepared datasets. The model is evaluated on signals acquired using a pure gamma source for different energy ranges. The results are compared with those obtained by TTT_{ratio} algorithm which validate the outperforming of the trained model. Finally, the article concludes by summarizing the main contributions and limitations of this labeling process (Section 6).

2. Experimental configuration

2.1. Tof setup

Time of flight (ToF) is a technique used to discriminate and label neutron and gamma-ray signals. This method relies on the speed difference between gamma-rays and neutrons to discriminate them, considering the gamma-ray is faster than the neutron. Nevertheless, acquired labeled datasets often contain mislabeled samples, which have various origins, such as the overlap between the gamma and neutron arrival time distributions and natural background radiations. These mislabeled samples have a penalizing impact on the evaluation of any discrimination approach.

The authors in [18] introduces an approach for minimizing the labeling error of ToF setups using a liquid scintillator. However, the implemented method cannot remove background events that coincidentally contribute to peaks in the ToF distribution. An alternative method for improving the precision of ToF measurements with liquid scintillator involves the use of an optimization algorithm to identify the time interval within the ToF distribution that has the lowest number of mislabeled samples [19]. Both approaches generated training and validation datasets of ML models presented in [20,21], respectively. In this study, the proposed method to reduce the error involves combining the results of ToF and TTT_{ratio} discrimination algorithm. By using this approach, mislabeled samples from the entire ToF distribution of the acquired dataset can be detected and removed, as shown by the results obtained in Section 4.

The experimental ToF setup involves two detectors separated by a distance L (50 cm), as illustrated in Fig. 3. The radiation source is placed in front of the start detector. When the oscilloscope identifies the detection of radiations at both detectors and the time between the two identifications is less than a preset time threshold, it records two signals corresponding to the radiation detected by each detector. Neutron and gamma-ray signals of the stop detector can be distinguished by the time of flight between the two detectors, which is calculated from the time duration between the peaks of both recorded signals. The components that we used to implement this setup are (Fig. 4):

- Start scintillator: EJ200 non-discriminating plastic scintillator made by Eljen Technology. This scintillator is not able to discriminate between neutrons and gamma-rays.
- Stop scintillator: EJ276 discriminating plastic scintillator used in the standard setup chain implemented in Section 2.2.

The acquisition was carried out with identical settings of the measurement chain implemented in Section 2.2, using the same PMT model and radiation source. The maximum time between triggering of the start and stop detectors is 60 ns.

It should be highlighted that the experimental results obtained from this ToF setup showed a significant percentage of pile-up events within the collected dataset. Thus, an offline digital detection method described in Section 3 was implemented to remove these events.

2.2. Experimental setup

The proposed labeling pipeline requires gamma-ray and mixed neutron/gamma-ray datasets for the labeling and generating synthetic pile-up signals, as explained in Sections 3 and 4. These datasets were acquired by the experimental configuration shown in Fig. 5. The scintillator is coupled to the PMT which is linked to the digitizer. The radiation source is placed at a given distance from the scintillator. The main components of this experimental set-up shown are:

- Scintillator: EJ276 discriminating plastic scintillator made by Eljen Technology. Its discrimination ability depends on the energy level of the detected ray, the lower the energy, the harder the discrimination.
- Photomultiplier: PMTETL9821 made by ET Enterprises which is supplied by 1700 V.
- Digitizer: LeCroy WAVERUNNER 640Zi with 8 bits vertical resolution.
- Radiation source: ^{252}Cf which is simultaneously a source of neutrons and gamma-rays and ^{60}Co which is a pure source of gamma-rays.

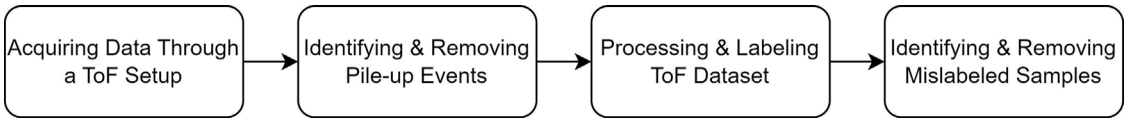

Fig. 2. The main steps of the proposed labeling pipeline.

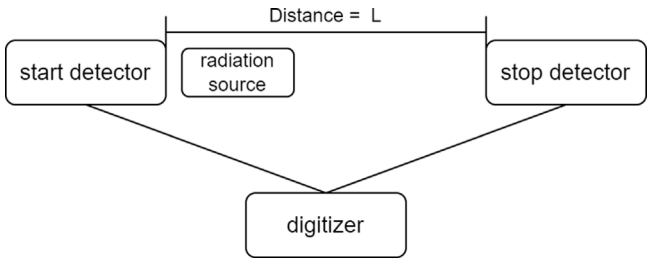

Fig. 3. Diagram representing the configuration of ToF experiment.

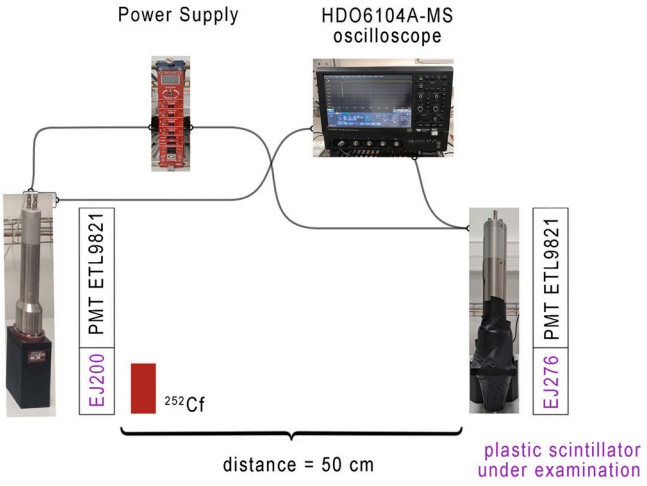

Fig. 4. Implemented ToF experiment.

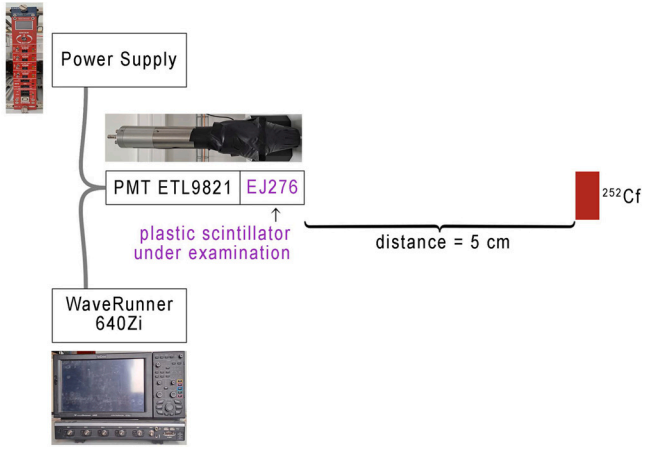

Fig. 5. The key components of the standard experimental setup.

The starting point of each signal is considered as the time when the signal reaches 10% of its maximum value. However, some signals contain background and electronic noises that have an intensity equal to or higher than this threshold. They sometimes appear at the beginning of the acquisition before several to tens nanoseconds from the actual starting point of the signal. To avoid this bias, the rising time mode of all acquired signals is computed. Thereafter, the search for the starting point of each signal is linked between the time of its maximum value and twice the average rise time.

The acquisition parameters were set to a triggering threshold of 60 mV, a sampling frequency of 5 GHz, a time window of 200 ns, and a V_{pp} of 3.2 V. A duration of 100 ns was assigned to the signal from its identified starting point, while the baseline was given a length of 50 ns.

The next step in the proposed labeling pipeline after the acquisition is identifying and removing the pile-up events obtained in the acquired ToF setup. Next section explains the method we proposed to detect and remove these events.

3. Pile-up detection and evaluation

Pile-up is a phenomenon that can occur when measuring signals with non-zero durations, such as neutrons and gamma-rays, whose arrival times follow a Poisson distribution. This event occurs when more than one signal is detected within the recorded duration, resulting in the detection of multiple local peaks in the overall acquired signal (Fig. 6(a)). These events are usually detected and rejected using a dedicated electronic system [22]. Nevertheless, some of them may be missed in the implemented ToF setup due to its coincidence acquisition characteristic and natural background radiations. As a result, an offline method is necessary to process these events and obtain a reliable datasets for neutron/gamma classification. Furthermore, evaluating the performance of the detection method can be challenging, as pile-up events in the acquired dataset cannot be easily identified. Therefore, a method for synthesizing pile-up events must be included in the evaluation process to assess the detection performance.

The performance of a pile-up detection algorithm is measured by determining its detection error, which is the percentage of undetected signals in a dataset consisting exclusively of pile-up events. Detecting pile-up events becomes more challenging as the time difference between the arrival of the two contributions within an event becomes smaller. Consequently, the evaluation must take this factor into account to identify the minimum threshold at which the detection error remains within an acceptable range. In our research, we considered a detection error of less than 1% to be acceptable.

3.1. Detection method

There are various algorithms available for handling digital detection of pile-up events. These include fitting [23,24] and deconvolution [25] methods, as well as an approach based on the first-order derivative [26]. Recently, a ML model has been developed that can simultaneously classify neutron, gamma-ray, and pile-up events of a liquid scintillator [13]. Another method for detecting pile-up events in germanium detectors has also been proposed, which leverages the relatively long signal length (in microseconds) to identify them [27].

The pile-up detection method implemented in this work to clean up the datasets acquired by ToF setup is inspired by the work of authors in [28]. The method is based on the cross-correlation between the output signal of the detector and a predefined Gaussian kernel. Cross-correlation measures the similarity between two vectors over time and the shape of an output signal produced by an organic scintillator is similar to the shape of a Gaussian window. This means that each peak in the cross-correlation output could indicate an event in the acquired signal. However, a Gaussian window that is too wide will cause the

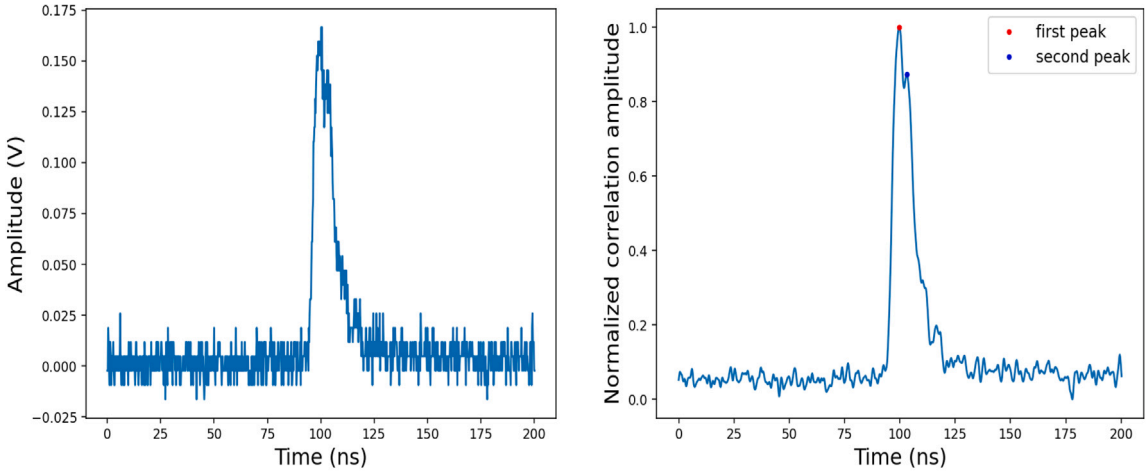

(a) A pile-up event (b) Correlation output

Fig. 6. Real detected pile-up event before and after the correlation with Gaussian kernel.

peaks of two closely occurring events to merge together. Conversely, a narrow window will result in detecting most signals as pile-ups, since any noise peak can be similar to the created narrow kernel and be identified as a pulse peak.

The optimal width of the kernel window depends on the standard deviation used to create the kernel and the number of points in the kernel array. In the presented case, the kernel size is the same as the signal length and the standard deviation should be adjusted to find its optimal value. The tuning can be done by gradually decreasing the standard deviation until the algorithm starts to misidentify the majority of the signals in a collected dataset as pile-ups. In other words, the optimal value is the point at which decreasing the standard deviation further would lead to a substantial misidentification of actual signals, while increasing it would lead to a considerable number of misidentified pile-up events. In the presented case, the obtained optimal value of the standard deviation was equal to 4. The first four lines of algorithm 1 summarize these steps. However, it should be noted that using the optimal standard deviation value obtained may misidentify some signals as pile-up events. The objective of this detection method is to prepare clean neutron gamma datasets, and the performance in terms of counting rate is not a concern.

After the correlation, in line five of algorithm 1, the peaks in the obtained output are detected using the implemented *find_peaks* function in *scipy* library in python. The function finds all local maximum by a simple comparison of neighboring values. Some of the detected peaks refer to noise signals. Therefore, by specifying conditions for a peak's properties, a subset of the detected peaks can be selected (Fig. 6(b)). These properties are width, amplitude, and the distance between two peaks. Finally, if the number of peaks that are found is higher than one, the acquired signal is considered as a pile-up.

Algorithm 1: Pile-up detection.

```
0: function pile − up − detection(signals)
1: sigma = obtainedoptimalvalue
2: window = Gaussian(length(signal), sigma)
3: corr = correlate(signal, window)
4: corr = (corr-min(corr))/(max(corr)-min(corr))
5: index_peaks = find-peaks (corr, high, width, distance)
6: if length(index_peaks > 1) then
7:     pile − up − event = 1
8: else
9:     pile − up − event = 0
10: end if
11: return pile − up − event
```

3.2. Evaluation of the detection method

To evaluate this detection method, a synthetic pile-up dataset is generated using real signals acquired using the setup explained in Section 2.2, where the radiation source is ^{252}Cf. A synthetic pile-up event is created by selecting randomly two acquired signals, shifting the second one, then adding them together. The shifting was determined by *arrival time difference* parameter which can be assigned to a constant or random value within a given predefined time interval. The shape of a created pile-up signal is quite realistic and similar to the shape of a real pile-up event. This is because the photomultiplier (PMT) current is proportional to the incident radiation fluxes magnitude which are linearly added when multiple radiations are detected in the same time window of the acquisition [29]. Moreover, this method allows us to precisely control the temporal arrival difference between the two rays of a synthetic pileup event. Therefore, the detection error can be evaluated according to the variation of this parameter. Table 1 summarizes the results of this evaluation, where the value of *arrival time distance* were adjusted between 5 and 15 ns. For each value, the execution was repeated 10 times, each time 100000 pile-up signals were generated.

The minimum *arrival time difference* required to keep the error less than 1% is 14 ns, meaning the proposed detection method can accurately identify a signal as a pile-up event if the second contribution arrives 14 ns after the first one. This does not imply that the method cannot detect pile-up events with a shorter arrival time difference between their two rays. Nonetheless, as indicated in Table 1, the likelihood of detection decreases when the distance between the two arrival times is less than this threshold. These results show that the simple implemented detection method with a single tuning parameter (standard deviation of the Gaussian kernel) is adequate to clean up pile-up events from the signals acquired by the ToF setup with a satisfying level of performance.

Finally, the obtained optimal value of the standard deviation of the Gaussian kernel was used to apply the algorithm on the datasets obtained by the ToF acquisition chain. The percentage of the detected pile-up events was 8.8% of the signals. This relatively high percentage validates the importance of their offline detection.

Table 1
Pile-up detection error (%) according to arrival time distance (nanoseconds) between the two contributions in a pile-up event.

Arrival time difference (ns)	5	6	7	8	9	10	11	12	13	14	15
Detection error	77.6%	66.5%	44.2%	29.8%	22.8%	17.1%	10.2%	3.9%	1.1%	0.6%	0.5%

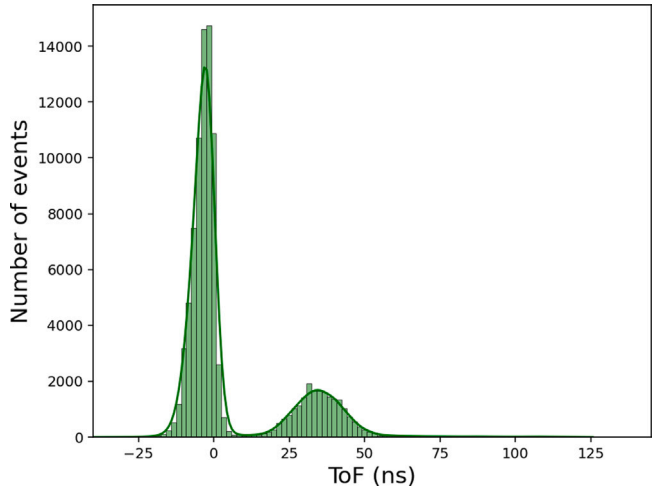

Fig. 7. Time-of-Flight Distribution.

4. Signal labeling

The presented labeling strategy combines the results of the ToF and TTT_{ratio} algorithm to identify and remove the mislabeled samples in the ToF setup.

4.1. Processing & labeling ToF dataset

The obtained ToF distribution of the remaining signals is illustrated in Fig. 7. The figure shows that the data contains two main classes. The left and right distributions are respectively corresponding to gamma-rays and neutrons. As gamma-rays are faster than neutrons, their ToF values are lower. However, the two ToF regions contain mislabeled gamma and neutron samples as we mentioned in Section 1. In Section 4.3, we will work on reducing the percentage of these events using the proposed labeling method.

It is worth mentioning that the obtained average ToF value of the neutron class (37 ns) is compatible with the expected value of the theory. This value is equal to 35.7 ns, considering the experimental set-up previously described. It can be computed by considering that the distance between the two detectors is equal to 50 cm and the mode energy of the neutrons emitted by the ^{252}Cf is 1 MeV which corresponds to a speed equal to 1.4 cm/ns [30]. Concerning the negative average ToF value of the gamma signals (−3.82 ns) is due to the difference response time of two detectors and the time resolution of the digitizer, since the speed of gamma is approximately equal to the speed of light in the air.

The samples located at the extremes of each class's distribution are primarily either mislabeled or irrelevant background events. Moreover, the region lying in between the two distributions is associated with significant uncertainty in classification. Therefore, in order to ensure accurate classification of acquired signals based on ToF parameter and to obtain well-labeled datasets, it is necessary to eliminate these samples. This can be done through the following steps:

1. Separate the detected radiations into two classes by applying the K-mean algorithm [31], taking the ToF values of the signals as input. The effectiveness of this method is illustrated in Fig. 8(a), which how the data are well-separated into two classes.
2. Calculate the ToF mean (μ) and standard deviation (σ) of each cluster.
3. Remove signals in each cluster i, if its ToF value is:

   - $ToF_{signal} > \mu_i + \beta * \sigma_i$

   or

   - $ToF_{signal} < \mu_i - \beta * \sigma_i$

   μ_i and σ_i are the mean and the standard deviation of cluster i.

The percentage of removed signals is inversely proportional to β. Moreover, the ToF distributions of both classes follow the Normal distribution. Therefore, by setting β to 3, 0.2% of the signals of each distribution are removed (Fig. 8(b)). In this way, the neutron and gamma clusters are ensured to be well separated with a low percentage of rejection.

4.2. Tail-to-total integral ratio

At the exit of a scintillation process on a organic scintillator, neutron signals are slightly longer than gamma rays. TTT_{ratio} algorithm takes benefit of this difference in the decay time to differentiate both contributions. The TTT_{ratio} of each signal $f(t)$ is computed using the following equation

$$TTT_{ratio} = \frac{Q_{tail}}{Q_{total}} \tag{1}$$

where $Q_{tail} = \int_{t_{short}}^{t_{long}} f(t)$ and $Q_{total} = \int_{0}^{t_{long}} f(t)$

The amplitude values of a signal are directly proportional to the detected radiation energy [29]. Therefore, this energy can be represented by the value of Q_{total}. The optimal values of the tuning parameters (t_{long} and t_{short}) are obtained by applying the optimization algorithm [32] on the dataset used to create the synthetic pile-up signals, where the obtained optimal values are respectively 18 ns and 100 ns.

This algorithm is applied on the dataset acquired by the ToF setup. Fig. 9 illustrates the two-dimensional graphical representation of the obtained distribution of TTT_{ratio} as a function of the total energy (Q_{total}). We can distinguish two main clusters. The overlapping between both of them shows the difficulty of the TTT_{ratio} algorithm to discriminate all signals, especially for relatively low energy radiations. Choosing one TTT_{ratio} threshold to classify the signals will lead to a significant number of mislabeled samples. Next section explains how this issue is treated. Furthermore, the TTT_{ratio} of the gamma-rays emitted by the cobalt (^{60}Co) source is calculated for use in the labeling strategy in the next section.

4.3. Labeling strategy

Fig. 10(a) shows the 2d graph of TTT_{ratio} according to total energy for signals labeled as neutron by ToF parameter. The figure contains two main clusters that represent true and mislabeled neutron radiations. To separate them and obtain a clean neutron dataset, a convenient $TTT_{NeutronThreshold}$ must be chosen. The TTT_{ratio} distribution of both clusters in Fig. 11 reveals two peaks corresponding to each cluster. $TTT_{NeutronThreshold}$ is chosen to be equal to the TTT_{ratio} value of the first peak plus half-width at half maximum (Fig. 10(a)). The ToF distribution of the removed samples is approximately similar to the original ToF distribution of the neutron cluster. Thus, with this approach, even background events that contribute to the peaks in the ToF spectrum can be removed.

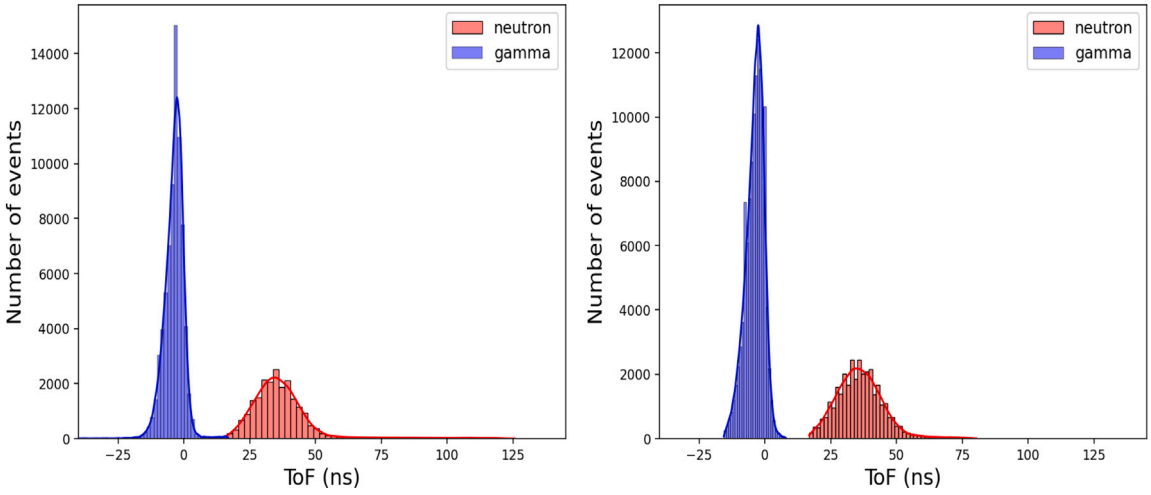

(a) ToF distribution of signals labeled by K-mean.

(b) ToF distribution for β equal to 3.

Fig. 8. Labeling of ToF output vector by K-mean algorithm.

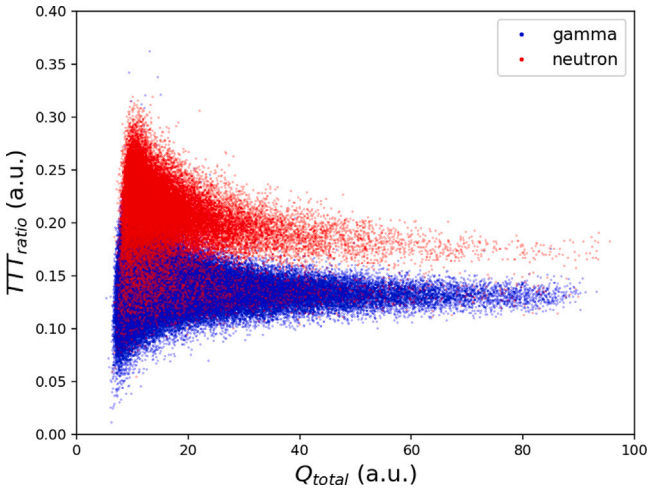

Fig. 9. TTT_{ratio} according to the total energy for signals of ToF setup.

It is important to note that it is uncertain that all background events can be identified by this method, and some neutron events may be misclassified. Furthermore, the removed signals may contain true neutron samples. Nevertheless, the performance of neutron counting rate is not a parameter of interest for this work.

Concerning the signals labeled as gamma-rays, the TTT_{ratio} distribution according to total energy has one main cluster (Fig. 10(b)). In other words, the contamination by mislabeled samples is relatively low. In order to increase the labeling accuracy, a $TTT_{GammaThreshold}$ is defined, which is calculated based on the normally distributed TTT_{ratio} obtained from a pure gamma dataset emitted by ^{60}Co (Fig. 12), by adding three times the standard deviation ($3 * \sigma_{\gamma_{TTT}}$) to the mean ($\mu_{\gamma_{TTT}}$). Consequently, the rejection rate is approximately equal to 0.5%.

Finally, at the end of this labeling pipeline, four datasets can be obtained. It should be emphasized that the primary objective of the proposed labeling process is to create an authentic dataset for neutrons. Gamma-ray signals can be obtained directly from gamma sources, such as ^{60}Co or ^{137}Cs.

1. neutron: signals are labeled as neutron using the proposed strategy.
2. gamma: signals are labeled as gamma using the proposed strategy.
3. mislabeled-neutron: signals classified as gamma by TTT_{ratio} method and neutron by ToF technique.
4. mislabeled-gamma: signals classified as neutron by TTT_{ratio} method and gamma by ToF technique.

Neutron and gamma datasets will be used to train the ANN model proposed in Section 5.

5. ANN model

5.1. Implementation

First, 165000 signals are acquired using the ToF setup previously described in Section 2.1. Then, pile-up events are detected and removed using the proposed detection method where the percentage of these events in the dataset is equal to 8.8%. The remaining signals are labeled using the strategy proposed in Section 4.3. The size of the obtained neutron and gamma datasets is respectively equal to 29600 and 117600 signals.

In order to explore the ability of a ML model to discriminate neutron/gamma radiations with plastic scintillator, an ANN model proof of concept is trained on the prepared data. The type of model is Multilayer Perceptron (MLP) Neural Network. The number of layers is equal to four:

1. An input layer has 500 neurons which is the number of points representing a signal.
2. Two hidden layers of 32 neurons each.
3. An output layer has one neuron which is the probability of a signal to be a neutron or gamma.

The data set is separated into 80% for the training and 20% for the validation. Binary cross-entropy and Adam algorithm are respectively the chosen loss function and optimizer algorithm. The number of epochs, waiting epochs, and batch size are assigned to 200, 10, and 16 respectively. ReLU and Sigmoid are respectively the activation functions of the hidden and last layers. The implementation is done using the Keras framework and Scikit-learn library.

The output of the model is a value between 0 and 1 which represents the probability that a radiation belongs to the neutron class. An output higher than 0.5 means that the ray is neutron, otherwise it is gamma.

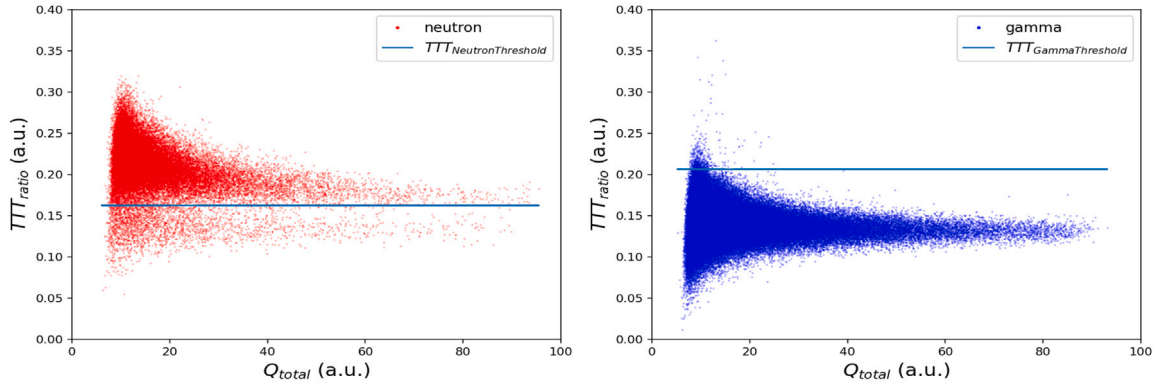

(a) neutron class (b) gamma class

Fig. 10. TTT_{ratio} according to total integral for each class of signals labeled by ToF parameter.

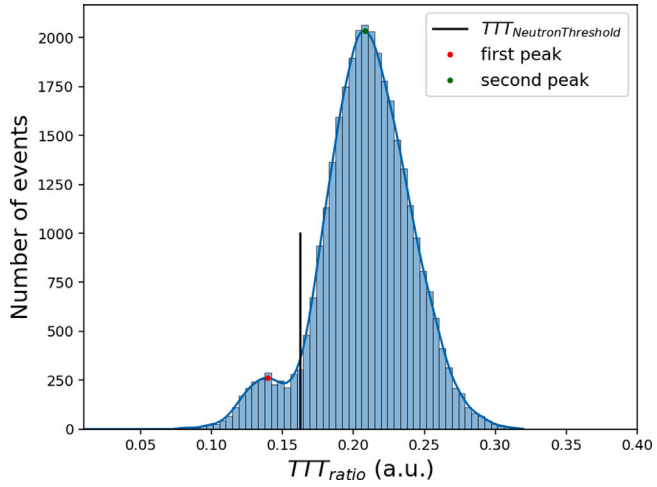

Fig. 11. TTT_{ratio} distribution of signals labeled as neutron by ToF.

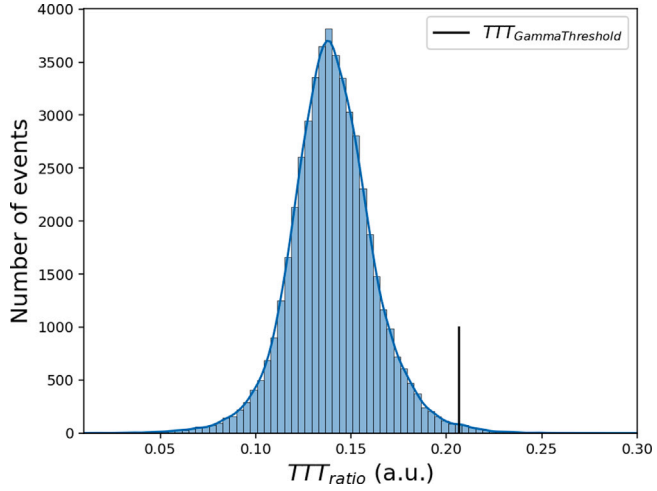

Fig. 12. TTT_{ratio} distribution of gamma-rays emitted by ^{60}Co.

In other word, 0.5 is usually used as a classification threshold. For the TTT_{ratio} discrimination algorithm, a chosen value of TTT_{ratio} that depends on the acquisition chain is used as a classification threshold.

Table 2
Confusion matrix of the validation data.

	Predicted neutron	Predicted gamma
True neutron	5443 (TP)	474 (FN)
True gamma	392 (FP)	23135 (TN)

5.2. Results

The accuracy achieved by this implemented model is 97% which is computed using the confusion matrix of the validation data represented in Table 2. The obtained True Positive Rate (TPR) is equal to 92%. This means that 80 samples from each 1000 neutrons will be classified as gamma rays. Moreover, for each 1000 gamma signals classified by the model, 20 false alarms are raised. In other words, the False Positive Rate (FPR) is equal to 2%.

The ratio of neutron rejection in ToF setup using the proposed labeling strategy is 9% (ratio of mislabeled neutrons to the total number of neutrons). 5% of these rejected samples are classified as true neutron by our ANN model. In other words, this ratio is reduced to 8.5% using our model.

Moreover, the FPR and TPR obtained by the trained model and TTT_{ratio} discrimination algorithm on the validation dataset at different classification thresholds shows that the first outperforms the second (Fig. 13). For the same FPR value, the TPR obtained by the trained model is higher.

Furthermore, in order to evaluate the behavior of the model when neutrons are not presented, the model is tested on a pure gamma dataset emitted by a ^{60}Co source for different energy ranges. Signals are acquired using the standard setup (Fig. 5). Then, the starting point of each raw sample is determined before being fed to the trained model to predict its type.

The radiation energy is represented by the total integral Q_{total} as we mentioned before. For each energy range, the FPR is computed and compared to the result obtained by the TTT_{ratio} discrimination algorithm. The obtained results are summarized in Table 3. Our model is more accurate than the TTT_{ratio} algorithm when treating $TTT_{NeutronThreshold}$ and less precise when choosing $TTT_{GammaThreshold}$. However, a lot of neutron samples will be missed by choosing $TTT_{GammaThreshold}$ when the detector is exposed to a source of mixed gamma/neutron radiations as proven by the experimental results of the labeling.

6. Contributions and limitations

The presented labeling pipeline can be used to prepared neutron dataset with any organic or inorganic scintillator. It can identify and

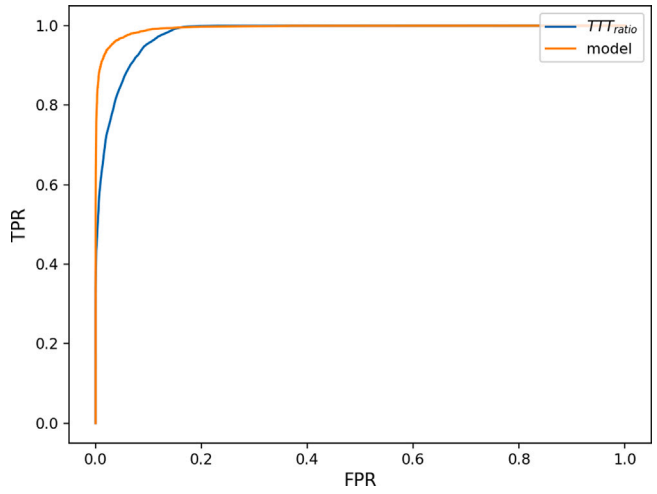

Fig. 13. FPR and TPR obtained by the trained model and TTT_{ratio} discrimination algorithm on validation data at different classification thresholds.

Table 3
FPR according to different energy ranges.

Total energy (Q_{total})	[5–10]	[10–20]	[20–30]
FPR of ANN	3.33%	1%	0.5%
FPR of $TTT_{GammaThreshold}$	1.7%	0.02%	0.0%
FPR of $TTT_{NeutronThreshold}$	32.7%	12.6%	6.21%

remove mislabeled samples in the entire ToF spectrum, including those that contribute to peak values. This process cleans ToF dataset from pile-up events, which can significantly impact experimental results and the conclusions extracted from them. This point is usually disregarded in the literature when ToF discrimination approach is employed to label the signals. Furthermore, the process can provide labeled datasets, even when the ability of discrimination of the implemented acquisition chain is relatively low. In the presented experimental setup, the obtained Figure of Merit is equal to 0.6 [33]. More accurate labeled dataset that have relatively lower energy range, can be obtained in a similar acquisition chain with higher discrimination ability, which is primarily dependent on SNR, as shown by the results obtained in [33].

The dependency on TTT_{ratio} discrimination algorithm is one main limitation of the proposed signal labeling method. Another limitation is the dependency on the sampling frequency and on the energy range of the incident radiations. The energy of the particle and its type determine both the distance it can travel and its speed. Therefore, when dealing with lower energy radiations, the distance between detectors needs to be reduced, resulting in lower ToF values for higher energy radiations. To detect these lower ToF values, the sampling rate must be increased. Moreover, compared to the traditional method, the ToF measurement chain is more complicated to be implemented, and the acquisition process takes longer time due to coincidence detection. This becomes particularly challenging as a large dataset is required to effectively identify the peak of mislabeled neutron dataset in the TTT_{ratio} distribution of the neutron signals labeled by ToF.

7. Conclusion and future developments

This article presents a pipeline to prepare clean and labeled neutron/gamma datasets in an organic scintillator. The initial step is to gather the dataset through an implemented ToF setup. The subsequent stage comprises detecting and removing pile-up events using a proposed and evaluated detection method. The remaining signals are then processed to decrease the number of background events and classified into neutron and gamma-ray classes. Finally, TTT_{ratio} discrimination algorithm is employed to reduce the percentage of mislabeled samples present in the obtained datasets. The article concludes with a discussion of the strengths and weaknesses of this labeling process.

Thereafter, an ANN proof of concept model is trained on the prepared datasets and it is evaluated on gamma pulses for different energy radiation ranges. The results are compared with those obtained by TTT_{ratio} discrimination algorithm. Our trained model in this approach outperforms the TTT_{ratio} method. For the same FPR value, the TPR obtained by the ANN model is higher.

In the future work, we will explore deeply the discrimination of neutrons and gamma-rays in an organic scintillator by different ML tools, such as supervised and unsupervised models. Different ML models and the state of the art algorithm (TTT_{ratio}) will be evaluated based on the variation of sampling frequency and the energy range of the incident radiations. Conducting discrimination at a lower energy level highlights the out-performance, while reducing the sampling rate minimizes the cost and size of embedded implementation. Training and validation datasets of the implemented models will be prepared by the proposed labeling process.

Declaration of competing interest

The authors declare that they have no known competing financial interests or personal relationships that could have appeared to influence the work reported in this paper.

References

[1] B. D'Mellow, M. Aspinall, R. Mackin, M.J. Joyce, A. Peyton, Digital discrimination of neutrons and γ-rays in liquid scintillators using pulse gradient analysis, Nucl. Instrum. Methods Phys. Res. A 578 (1) (2007) 191–197.

[2] J. Adams, G. White, A versatile pulse shape discriminator for charged particle separation and its application to fast neutron time-of-flight spectroscopy, Nucl. Instrum. Methods 156 (3) (1978) 459–476.

[3] S. Marrone, D. Cano-Ott, N. Colonna, C. Domingo, F. Gramegna, E. Gonzalez, F. Gunsing, M. Heil, F. Käppeler, P. Mastinu, et al., Pulse shape analysis of liquid scintillators for neutron studies, Nucl. Instrum. Methods Phys. Res. A 490 (1–2) (2002) 299–307.

[4] F. Brooks, Development of organic scintillators, Nucl. Instrum. Methods 162 (1–3) (1979) 477–505.

[5] T. Laplace, B. Goldblum, J. Bevins, D. Bleuel, E. Bourret, J. Brown, E. Callaghan, J. Carlson, P. Feng, G. Gabella, et al., Comparative scintillation performance of EJ-309, EJ-276, and a novel organic glass, J. Instrum. 15 (11) (2020) P11020.

[6] M. Grodzicka-Kobylka, T. Szczesniak, M. Moszyński, K. Brylew, L. Swiderski, J. Valiente-Dobón, P. Schotanus, K. Grodzicki, H. Trzaskowska, Fast neutron and gamma ray pulse shape discrimination in EJ-276 and EJ-276G plastic scintillators, J. Instrum. 15 (03) (2020) P03030.

[7] F. Ferrulli, N. Dinar, L.G. Manzano, M. Labalme, M. Silari, Characterization of stilbene and EJ-276 scintillators coupled with a large area SiPM array for a fast neutron dose rate detector, Nucl. Instrum. Methods Phys. Res. A 1010 (2021) 165566.

[8] M. Grodzicka-Kobylka, T. Szczesniak, M. Moszyński, K. Brylew, L. Swiderski, J. Valiente-Dobón, P. Schotanus, K. Grodzicki, H. Trzaskowska, Fast neutron and gamma ray pulse shape discrimination in EJ-276 and EJ-276G plastic scintillators, J. Instrum. 15 (03) (2020) P03030.

[9] G.F. Knoll, Radiation Detection and Measurement, John Wiley & Sons, 2010.

[10] E. TECHNOLOGY, PSD Plastic scintilator EJ-276 and EJ-276g, 2022, URL https://eljentechnology.com/images/products/data_sheets/EJ-276.pdf.

[11] H. Arahmane, E.-M. Hamzaoui, R. Moursli, Improving neutron-Gamma discrimination with stilbene organic scintillation detector using blind nonnegative matrix and tensor factorization methods, J. Spectrosc. 2019 (2019) 1–9, http://dx.doi.org/10.1155/2019/8360395.

[12] L.M. Simms, B. Blair, J. Ruz, R. Wurtz, A.D. Kaplan, A. Glenn, Pulse discrimination with a Gaussian mixture model on an FPGA, Nucl. Instrum. Methods Phys. Res. A 900 (2018) 1–7.

[13] C. Fu, A. Di Fulvio, S. Clarke, D. Wentzloff, S. Pozzi, H. Kim, Artificial neural network algorithms for pulse shape discrimination and recovery of piled-up pulses in organic scintillators, Ann. Nucl. Energy 120 (2018) 410–421.

[14] X. Yu, J. Zhu, S. Lin, L. Wang, H. Xing, C. Zhang, Y. Xia, S. Liu, Q. Yue, W. Wei, Q. Du, C. Tang, Neutron–gamma discrimination based on the support vector machine method, Nucl. Instrum. Methods Phys. Res. A 777 (2015) 80–84, http://dx.doi.org/10.1016/j.nima.2014.12.087, URL https://www.sciencedirect.com/science/article/pii/S0168900214015551.

[15] W. Zhang, W. Tongyu, B. Zheng, L. Shiping, Y. Zhang, Y. Zejie, A real-time neutron-gamma discriminator based on the support vector machine method for the time-of-flight neutron spectrometer, Plasma Sci. Technol. 20 (4) (2018) 045601.

[16] S. Pozzi, M. Bourne, S. Clarke, Pulse shape discrimination in the plastic scintillator EJ-299-33, Nucl. Instrum. Methods Phys. Res. A 723 (2013) 19–23.

[17] D. Fobar, L. Phillips, A. Wilhelm, P. Chapman, Considerations for training an artificial neural network for particle type identification, IEEE Trans. Nucl. Sci. 68 (9) (2021) 2350–2357.

[18] M. Aspinall, B. D'Mellow, R. Mackin, M. Joyce, N. Hawkes, D. Thomas, Z. Jarrah, A. Peyton, P. Nolan, A. Boston, Verification of the digital discrimination of neutrons and γ rays using pulse gradient analysis by digital measurement of time of flight, Nucl. Instrum. Methods Phys. Res. A 583 (2–3) (2007) 432–438.

[19] K.P. Lennox, P. Rosenfield, B. Blair, A. Kaplan, J. Ruz, A. Glenn, R. Wurtz, Assessing and minimizing contamination in time of flight basedvalidation data, Nucl. Instrum. Methods Phys. Res. A 870 (2017) 30–36.

[20] A.D. Kaplan, B. Blair, C. Chen, A. Glenn, J. Ruz, R. Wurtz, A neutron-gamma pulse shape discrimination method based on pure and mixed sources, Nucl. Instrum. Methods Phys. Res. A 919 (2019) 36–41.

[21] G. Liu, M. Aspinall, X. Ma, M. Joyce, An investigation of the digital discrimination of neutrons and γ rays with organic scintillation detectors using an artificial neural network, Nucl. Instrum. Methods Phys. Res. A 607 (3) (2009) 620–628.

[22] V.T. Jordanov, Deconvolution of pulses from a detector-amplifier configuration, Nucl. Instrum. Methods Phys. Res. A 351 (2–3) (1994) 592–594.

[23] S. Marrone, D. Cano-Ott, N. Colonna, C. Domingo, F. Gramegna, E. Gonzalez, F. Gunsing, M. Heil, F. Käppeler, P. Mastinu, et al., Pulse shape analysis of liquid scintillators for neutron studies, Nucl. Instrum. Methods Phys. Res. A 490 (1–2) (2002) 299–307.

[24] F. Belli, B. Esposito, D. Marocco, M. Riva, Y. Kaschuck, G. Bonheure, et al., A method for digital processing of pile-up events in organic scintillators, Nucl. Instrum. Methods Phys. Res. A 595 (2) (2008) 512–519.

[25] W. Guo, R.P. Gardner, C.W. Mayo, A study of the real-time deconvolution of digitized waveforms with pulse pile up for digital radiation spectroscopy, Nucl. Instrum. Methods Phys. Res. A 544 (3) (2005) 668–678.

[26] X. Luo, V. Modamio, J. Nyberg, J. Valiente-Dobón, Q. Nishada, G. De Angelis, J. Agramunt, F. Egea, M. Erduran, S. Ertürk, et al., Pulse pile-up identification and reconstruction for liquid scintillator based neutron detectors, Nucl. Instrum. Methods Phys. Res. A 897 (2018) 59–65.

[27] M. Nakhostin, Z. Podolyak, P. Regan, P. Walker, A digital method for separation and reconstruction of pile-up events in germanium detectors, Rev. Sci. Instrum. 81 (10) (2010) 103507.

[28] S. Lee, B. Park, Y. Kim, H. Myung, Peak detection with pile-up rejection using multiple-template cross-correlation for MWD (measurement while drilling), in: Robot Intelligence Technology and Applications 3, Springer, 2015, pp. 753–758.

[29] R.W. Engstrom, Photomultiplier Handbook, RCA Solid State Division. Electro Optics and Devices, 1980.

[30] J.F. Dicello, W. Gross, U. Kraljevic, Radiation quality of Californium-252, Phys. Med. Biol. 17 (3) (1972) 345–355, http://dx.doi.org/10.1088/0031-9155/17/3/301.

[31] J. MacQueen, et al., Some methods for classification and analysis of multivariate observations, in: Proceedings of the Fifth Berkeley Symposium on Mathematical Statistics and Probability, Vol. 1, no. 14, Oakland, CA, USA, 1967, pp. 281–297.

[32] C. Lynde, E. Montbarbon, M. Hamel, A. Grabowski, C. Frangville, G.H. Bertrand, G. Galli, F. Carrel, V. Schoepff, Z. El Bitar, Optimization of the charge comparison method for multiradiation field using various measurement systems, IEEE Trans. Nucl. Sci. 67 (4) (2020) 679–687.

[33] A. Hachem, A. Kanj, Y. Moline, G. Corre, C. Lynde, F. Carrel, Neutron/Gamma discrimination performance with plastic scintillator according to SNR, vertical resolution and sampling frequency, in: 2022 IEEE Nuclear Science Symposium (NSS), Medical Imaging Conference (MIC) and Room Temperature Semiconductor Detector (RTSD) Conference, 2022, forthcoming.